

See discussions, stats, and author profiles for this publication at: <https://www.researchgate.net/publication/261101325>

Synthesis of pH-Responsive Chitosan Nanocapsules for Controlled Delivery of Doxorubicin.

ARTICLE in LANGMUIR · MARCH 2014

Impact Factor: 4.46 · DOI: 10.1021/la4040485 · Source: PubMed

CITATIONS

3

READS

88

11 AUTHORS, INCLUDING:



Chih-Kuang Chen

Feng Chia University

23 PUBLICATIONS 337 CITATIONS

[SEE PROFILE](#)



Charles H Jones

Abcombi Biosciences Inc.

19 PUBLICATIONS 156 CITATIONS

[SEE PROFILE](#)



Yun Yu

State University of New York

11 PUBLICATIONS 187 CITATIONS

[SEE PROFILE](#)



Hanguang Zhang

University at Buffalo, The State University of N...

4 PUBLICATIONS 26 CITATIONS

[SEE PROFILE](#)

Synthesis of pH-Responsive Chitosan Nanocapsules for the Controlled Delivery of Doxorubicin

Chih-Kuang Chen,^{†,§} Qing Wang,[†] Charles H. Jones,[†] Yun Yu,[†] Hanguang Zhang,[†] Wing-Cheung Law,[‡] Cheng Kee Lai,[†] Qinghang Zeng,[†] Paras N. Prasad,[‡] Blaine A. Pfeifer,[†] and Chong Cheng^{*,†}

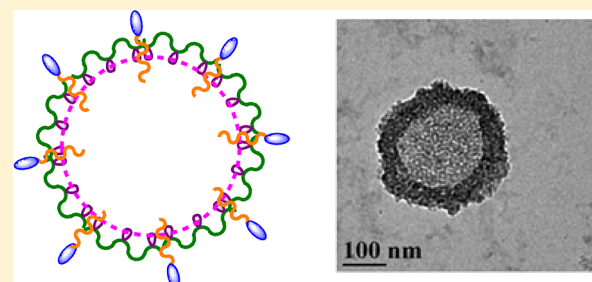
[†]Department of Chemical and Biological Engineering and [‡]Institute for Lasers, Photonics and Biophotonics, University at Buffalo, The State University of New York, Buffalo, New York 14260, United States

[§]Department of Fiber and Composite Materials, Feng Chia University, Taichung, Taiwan 40724, ROC

Supporting Information

ABSTRACT: Well-defined chitosan nanocapsules (CSNCs) with tunable sizes were synthesized through the interfacial cross-linking of *N*-maleoyl-functionalized chitosan (MCS) in miniemulsions, and their application in the delivery of doxorubicin (Dox) was investigated. MCS was prepared by the amidation reaction of CS with maleic anhydride in water/DMSO at 65 °C for 20 h. Subsequently, thiol–ene cross-linking was conducted in oil-in-water miniemulsions at room temperature under UV irradiation for 1 h, using MCS as both a surfactant and precursor polymer, 1,4-butanediol bis(3-mercaptopropionate) as a cross-linker, and D- α -tocopheryl poly(ethylene glycol) 1000 succinate as a cosurfactant.

With the increase in cosurfactant concentration in the reaction systems, the sizes of the resulting CSNCs decreased steadily. Dox-loaded CSNCs were readily prepared by *in situ* encapsulation of Dox during miniemulsion cross-linking. With acid-labile β -thiopropionate cross-linkages, the Dox-loaded CSNCs demonstrated a faster release rate under acidic conditions. Relative to free Dox, Dox-loaded CSNCs exhibited enhanced cytotoxicity toward MCF-7 breast cancer cells without any noticeable cytotoxicity from empty CSNCs. The effective delivery of Dox to MCF-7 breast cancer cells via Dox-loaded CSNCs was also observed.



INTRODUCTION

With cancer being the second leading cause of mortality worldwide, chemotherapy has emerged as one of the most common modalities employed to combat this disease.¹ A variety of anticancer drugs have been developed, but their clinical potential is hampered by poor water solubility, short circulation time, and severe off-target effects that result in systemic toxicity and poor antitumor efficiency.^{2,3} Consequently, with the advancement of nanotechnology, the applications of nanosized scaffolds for the delivery of anticancer drugs have been studied to tackle the aforementioned hurdles in chemotherapy.^{4–6} These scaffolds should possess various features, including nanoscopic dimensions, biodegradability, nontoxicity, stimuli responsivity, and manufacturing feasibility.^{7–10} In particular, the stimuli responsivity of scaffolds may allow the controlled release of anticancer drugs in tumor-specific conditions, leading to reduced systemic toxicity, and may permit higher maximum tolerated doses in repeated administrations. Because tumor tissue is slightly more acidic than normal tissue, scaffolds enabling the acid-triggered release of drug loading have attracted broad interest recently.^{11,12}

Chitosan (CS), a biopolymer composed of *N*-acetylglucosamine and glucosamine units, has been widely used as drug carrier because of its biocompatibility, biodegradability, non-toxicity, and low cost.^{13–17} Derived from chitin via deacetylation, CS possesses a pK_a value of around 6.5, which

significantly limits its water solubility under physiological conditions.¹⁸ Although the solubility of CS can be improved by reducing its molecular weight,¹⁹ chemical modification on the CS backbone through PEGylation, quaternization, sulfonation, or other chemical reactions has become the primary method of enhancing the solubility of CS-based materials at physiological pH.^{20–22} CS derivatives possessing amphiphilicity have been synthesized and utilized for the construction of micellar structures, which can be further employed for drug encapsulation. However, micelles can accommodate only small quantities of drug loading,^{23–26} and they also lack structural stability under dilution in the bloodstream.⁵ With significant structural stability, CS-based cross-linked particles have been successfully prepared by cross-linking in emulsion, coacervation, and microfluidic systems.^{14,27} However, it is difficult to obtain CS-based cross-linked particles with optimal sizes (10–100 nm) for enhanced permeability and retention (EPR) effects via these approaches.²⁸ Furthermore, glutaraldehyde is a commonly used cross-linker in these approaches, but it can react with amine-containing anticancer drugs.^{14,29,30} Additionally, the emulsion cross-linking synthesis of CS-based particles typically utilizes water-in-oil (W/O) emulsions and the

Received: October 18, 2013

Revised: February 15, 2014

Published: March 25, 2014



resulting particles can encapsulate only hydrophilic drugs, but most anticancer drugs are hydrophobic.

Relative to other types of CS-based drug-delivery vehicles, CS-based capsules with cross-linked structures possess both significant drug-loading capacity and remarkable structural stability and therefore have attracted significant interest.^{31–34} Because CS has a moderate surfactant effect and can form interfacial layers at water–oil interfaces to stabilize oil droplets via both electrostatic and steric effects,³⁵ emulsion-based cross-linking approaches have been utilized for the preparation of CS-based capsules. For instance, Chu and co-workers reported the cross-linking of CS microcapsules with acid-labile Schiff base cross-linkages through double emulsions using a microfluidic approach,³⁶ and these CS microcapsules exhibited an acid-triggered decomposition when the environmental pH dropped below 4.7. However, drug carriers with sizes smaller than 100 nm have shown an ability to reduce hepatic filtration, decrease blood clearance, and lower nonspecific protein adsorption. Accordingly, nanoscopic dimensions of drug carriers are required to avoid fast systemic clearance.³⁷ Thus, as compared to microcapsules, nanocapsules (NCs) as therapeutic carriers are generally more relevant to clinical applications.

Several types of CS-based NCs (CSNCs) have been reported, but the synthesis of well-defined stimuli-responsive CSNCs remains challenging. Landfester and co-workers reported the first examples of CSNCs, which were prepared by the oil-in-water (O/W) miniemulsion interfacial polyaddition cross-linking of CS using epoxide as a cross-linker.³⁸ However, these CSNCs could not exhibit the stimuli-triggered release of cargo because of the absence of stimuli-responsive macromolecular structures. Recently, stimuli-responsive pluronic-CS NCs have been reported by He and co-workers.³⁹ By the interfacial cross-linking of pluronic F127 and CS in O/W emulsions, these NCs exhibited dramatic thermally responsive size and wall-permeability changes between 4 and 37 °C based on the sol–gel transition of the pluronic copolymer. These thermally responsive NCs may have applications in the selective encapsulation and release of therapeutic agents at predetermined temperatures.

We are very interested in the synthesis and biomedical applications of polymeric NCs. As we reported previously, polylactide (PLA)-based NCs and polyelectrolyte NCs were prepared by miniemulsion-based cross-linking approaches.^{40–42} However, it is relatively expensive and time-consuming to prepare the precursors of these NCs, which require multistep synthesis. In this article, we report our recent studies of well-defined pH-responsive CSNCs. A miniemulsion interfacial cross-linking strategy was employed in the synthesis of these CSNCs via UV-induced thiol–ene chemistry.^{40,41} Because N-maleoyl-functionalized CS (MCS) that can be prepared from CS by a one-step reaction was used as the precursor of NCs, the overall synthesis efficiency of NCs in this study is much higher than that in our previous studies. Using CS as the major feedstock, the synthesis route in this study is also more sustainable and environmentally friendly. Moreover, the sizes of these CSNCs can be easily controlled by tuning the concentration of cosurfactant in miniemulsions. The CSNCs can readily encapsulate anticancer drugs during the miniemulsion cross-linking process, and relative to CS-based nanoparticles, these CSNCs possess a higher drug loading. With acid-labile β -thiopropionate cross-linkages,^{43,44} these CSNCs exhibited enhanced release behavior at acidic pH and demonstrated significant application potential in the delivery of

anticancer drugs through in vitro experiments. To the best of our knowledge, this is the first report that demonstrates the synthesis and acid-triggered release behavior of pH-responsive CSNCs.

EXPERIMENTAL SECTION

Measurements. All ^1H NMR spectra were recorded at 500 MHz on solutions in D_2O on a Varian INOVA-500 spectrometer maintained at 25 °C. The average hydrodynamic diameters (D_h) and zeta potentials of CSNCs were measured by dynamic light scattering (DLS) on a nano-ZS90 (Malvern, Inc.) in water at 25 °C, and all experiments were conducted using a 4 mW, 633 nm HeNe laser as the light source at a measuring angle of 90° fixed with respect to the incident laser beam. The correlation decay functions were analyzed by the cumulant method coupled with Mie theory to obtain the volume distribution. All samples were passed through a 450 nm low-protein-binding hydrophilic LCR (PTFE) membrane filter (Millex-LCR, Millipore) to provide a dust-free process before DLS measurements were made. TEM images were acquired using a JEOL 2010 microscope. TEM samples were prepared by dip coating a 300 mesh carbon-coated copper grid with a dilute sample solution of 1.5 mg/mL, followed by staining using ruthenium tetroxide for 1 day. The concentration of Dox was determined using a Shimadzu 3101PC UV-vis–NIR scanning spectrophotometer based on the characteristic UV-vis adsorption of Dox at 490 nm. Cell imaging was conducted by using a Leica TCS-SP2/AOBS confocal microscope equipped with excitation laser lines of 405, 442, 458, 476, 488, 496, 543, and 633 nm and capable of spectral detection in the range of 400–720 nm. All of the confocal images were taken under the same conditions (the parameters of photodetector gain, pinhole size, and exposure time were kept constant).

Materials. CS_{5k} (10% acetylation; MW = 5 kDa; soluble in deionized water), D- α -tocopheryl polyethylene glycol 1000 succinate (TPGS), and maleic anhydride (MA, 99%) were purchased from Sigma-Aldrich. Dimethyl sulfoxide (DMSO, HPLC), chloroform (HPLC), acetone, and methanol (HPLC) were purchased from Fisher Chemical. 2,2-Dimethoxy-2-phenylacetophenone (DMPA, 99+ %) was purchased from Acros Organics. 1,4-Butanediol bis(3-mercaptopropionate) (98%) was purchased from TCI. Doxorubicin hydrochloride (Dox-HCl, 98–102%) was purchased from Sigma and converted to water-insoluble Dox following an established protocol.⁴⁵

Synthesis of N-Maleoyl Chitosan (MCS). A mixed solution (50 mL) composed of deionized water (15 mL) and DMSO (35 mL) was prepared to dissolve CS_{5k} (250 mg; NH_2 = 1.4 mmol). After the solution was heated to 65 °C, an acetone solution (10 mL) of MA (1.0 g, 10.2 mmol) was added dropwise over 40 min. The reaction mixture was stirred for 20 h at 65 °C, followed by precipitation in acetone (800 mL). After filtration, the resulting polymer was washed with methanol via five centrifugation cycles to remove impurities (5 × 20 mL). After the solvents were completely removed in vacuum, the pure MCS, appearing as a pale-yellow solid, was collected (yield: 87%). By ^1H NMR analysis, the degree of substitution of the N-maleoyl functional group relative to glucosamine-based units on the CS backbone was 16%, corresponding to a M_n^{NMR} of 5.5 kDa.

Preparation of CSNCs. In a 10 mL vial, a chloroform solution (0.112 mL) containing 1,4-butanediol bis(3-mercaptopropionate) (1.17 mg, 0.0088 mmol of thiol groups) and DMPA (1.13 mg, 0.0044 mmol) was added to 3.5 mL of MCS aqueous solution (9.6 mg of MCS, 0.0087 mmol of the maleoyl group) with a given concentration of TPGS (0–0.9 mM). The O/W miniemulsion was prepared after 20 min of ultrasonication of the mixture using a 68 μm microtip amplitude. In continuous mode, ultrasonication was conducted using a 150 series Digital Sonic dismembrator (Fisher Scientific) equipped with an SLP microtip (0.08 in. diameter, Brason Ultrasonics). Subsequently, a thiol–ene cross-linking reaction was induced by UV irradiation of the miniemulsion for 1 h at room temperature. The UV irradiation was carried out using a UVGL-58 hand-held UV lamp (6 W, 0.12 A, $\lambda_{\text{max}} = 365 \text{ nm}$). After removing

chloroform by simple evaporation using a rotavapor at room temperature, an aqueous solution of CSNCs was obtained.

Preparation of Dox-Loaded CSNCs (Dox-CSNCs). Dox-CSNCs were prepared following the procedure for the preparation of CSNCs, except that hydrophobic Dox (0.8 mg) was dissolved in the chloroform solution before the emulsification process and extracted using chloroform as a solvent (5×2 mL) after cross-linking. After the chloroform was completely removed, the drug-loading amount and encapsulation efficiency of Dox-CSNCs were measured on the basis of the UV-vis absorbance of Dox at 490 nm.

In Vitro Dox Release from Dox-CSNCs. In vitro Dox release experiments were conducted using a dialysis procedure. An aqueous solution (3.5 mL) of Dox-CSNC-2 or Dox-CSNC-3 was added and sealed in a dialysis bag (MWCO = 3500 Da). Then the dialysis bag was immersed in 46.5 mL of 10 mM phosphate buffer solution (pH 7.4 or 5.5). The dialysis system was kept at 37 °C using an oil bath with a gentle stirring. At predefined time intervals, aliquots in the buffer solution were withdrawn, followed by refilling equal amounts of fresh buffer solutions to keep a constant total volume of the release medium. The amounts of Dox in the release medium were quantified in terms of its UV-vis absorbance at 490 nm, and the cumulative drug release percentages were recorded at given time intervals.

MTS Assay for Cell Viability. An MTS (3-(4,5-dimethylthiazol-2-yl)-5-(3-carboxymethoxyphenyl)-2-(4-sulfophenyl)-2*H*-tetrazolium, inner salt, Promega) assay was performed to evaluate the cytotoxicity of free Dox, Dox-CSNC-3, and CSNC-3 in MCF-7 cells (breast cancer cells). Following previously established procedures and using an untreated control,⁴¹ various concentrations of CSNC-3, free Dox, and Dox-CSNC-3 were exposed to MCF-7 cells for 48 h. The desired Dox concentrations of Dox-CSNC-3 for each well were obtained by adding the required amounts of Dox-CSNC-3 solution with a predetermined Dox concentration in the culture medium. The Dox concentration of Dox-CSNC-3 solution was determined on the basis of the UV absorbance of Dox at 490 nm. After 48 h of incubation, sample solutions were removed, and the wells were washed twice with fresh PBS to eliminate the intercellular presence of Dox and to minimize the interference from Dox adsorption in cytotoxicity analysis. Then, 10 μ L of the MTS reagent with 100 μ L of the fresh culture medium was added to each well and thoroughly mixed. The absorbance of formazan (produced by the cleavage of MTS by dehydrogenases in living cells) is directly proportional to the number of live cells. One hour later, the absorbance of each well at 490 nm was measured using a multiwell plate reader. Assays were performed in quadruplicate, and the results were presented in the form of average \pm standard deviation (the viability of untreated cells was assigned as 100%).

Confocal Imaging. The day prior to imaging experiments, MCF-7 cells were seeded on a square glass coverslip in 35 mm cell culture dishes at 40–50% confluence. For Dox delivery experiments, culture dishes were treated with a 62 μ L solution of Dox-CSNC-3 (2.8 mg/mL) with the final concentration of Dox equal to 20 μ M. The samples were then cultured at 37 °C in a humidified atmosphere containing 5% CO₂ for 1 and 4 h, followed by confocal analysis.

RESULTS AND DISCUSSION

Synthesis and Characterization of MCS. MCS was selected as the precursor of water-dispersible CSNCs prepared through thiol–ene miniemulsion cross-linking because it possesses *N*-maleoyl alkene unsaturation and enhanced aqueous solubility. It was synthesized by the amidation reaction between the primary amines of CS and MA (Scheme 1). Because the solubility of CS increases with the decrease in molecular weight,¹⁹ CS_{Sk} (MW = 5 kDa, 10% acetylation) was chosen in this study. The reaction was conducted in a water/DMSO mixed solvent at 65 °C for 20 h ($[\text{NH}_2]_0/[\text{MA}]_0 = 1:7$). The resulting MCS was obtained in 87% isolation yield relative to CS_{Sk}. Its chemical structure was verified by ¹H NMR analysis (Figure 1a), and the presence of *N*-maleoyl alkene protons of MCS at 5.82 and 6.27 ppm indicates the success of

Scheme 1. Synthesis of MCS

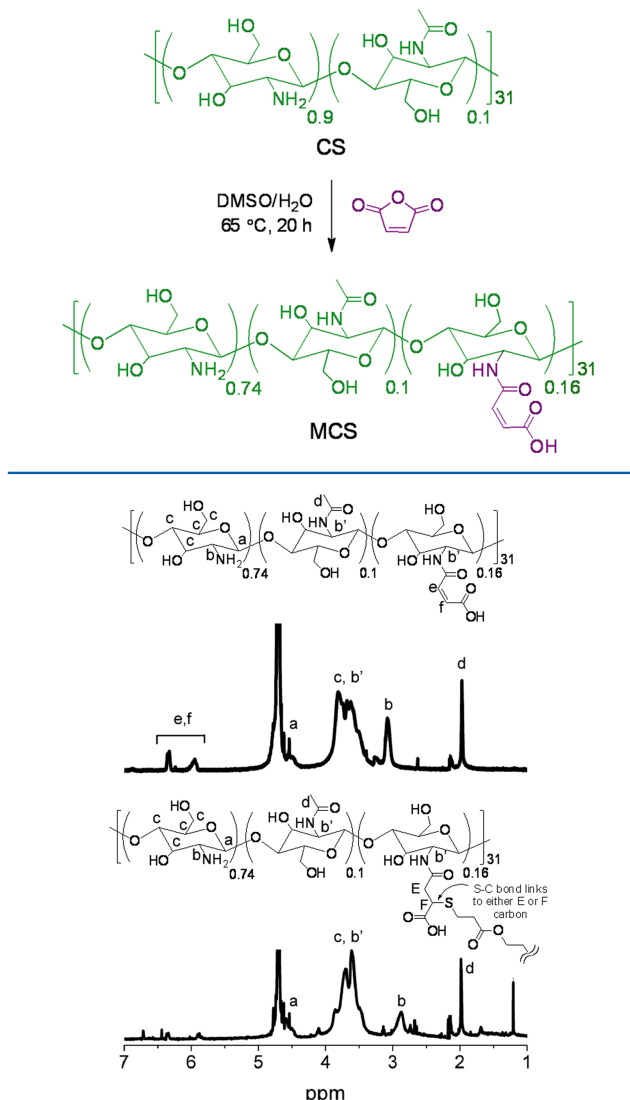
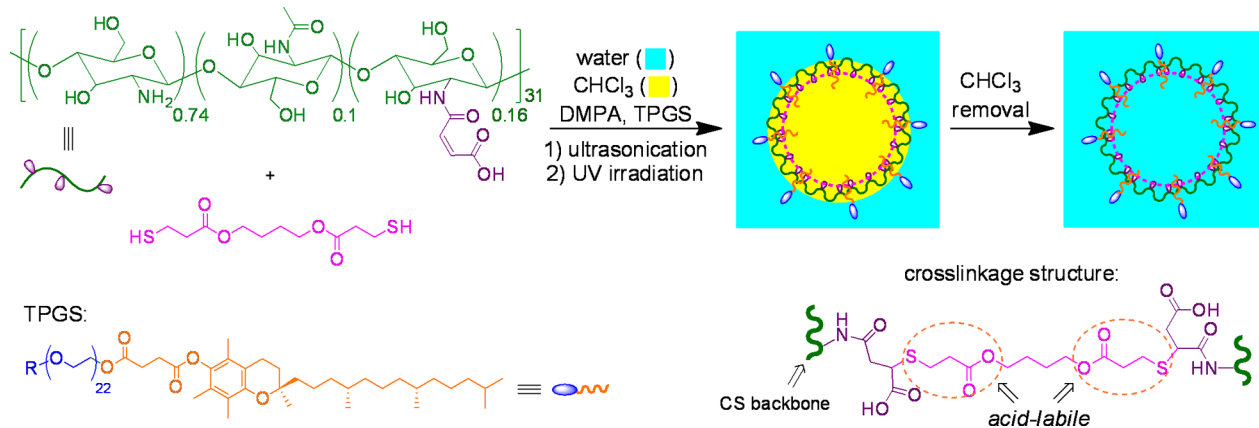


Figure 1. 500 MHz ¹H NMR spectra of (top) MCS and (bottom) CSNC-3 in D₂O.

the *N*-maleoyl modification of CS.⁴⁶ By comparing the resonance intensities of the *N*-maleoyl protons with those of the CH protons at the α position of the amine of the glucosamine-based repeat units at 3.04 ppm,⁴⁷ 16% substitution of *N*-maleoyl functionality on the CS backbone was deduced. The low degree of substitution can be attributed to the hydrolysis of MA in the reaction medium in which water was employed to assist the dissolution of CS. A control experiment was conducted under the same reaction conditions except in the absence of CS, and ¹H NMR analysis of the reaction mixture showed the complete conversion of MA to maleic acid by hydrolysis. Moreover, according to the literature, higher degrees of maleation can be obtained from the reaction systems using nonaqueous reaction media.^{46,48}

Synthesis and Characterization of CSNCs. Well-defined CSNCs were synthesized through a UV-induced thiol–ene miniemulsion interfacial cross-linking strategy.^{40,49} Having moderate surfactant efficacy, CS has been used as a stabilizer for the preparation of O/W emulsions.³⁵ In particular, it has been reported that only the use of low-molecular-weight CS

Scheme 2. Preparation of CSNCs via Miniemulsion Interfacial Cross-Linking

can reduce the surface tension of aqueous solutions.³⁸ Similar to CS, MCS also possesses amphiphilic properties and therefore was used as both a surfactant and a reactant for the preparation of CSNCs (Scheme 2, Table 1). To introduce acid-

version of *N*-maleoyl groups can be ascribed to the low transparency of the miniemulsion reaction system. Without high transparency, the miniemulsion could not allow efficient UV light penetration, thereby reducing the extent of reaction in cross-linking.⁴⁰

With the presence of TPGS as a cosurfactant but other conditions unchanged, the synthesis of CSNCs was further studied. In principle, in the presence of cosurfactant in miniemulsion systems, interfacial tension can decrease further to facilitate the increase in the interface area per unit volume and the formation of smaller oil droplets, thereby increasing the transparency of miniemulsions. As a result, relative to CSNC-0, CSNCs with smaller sizes were obtained. When the concentration of TPGS in the miniemulsion solution increased from 0.18 to 0.54 mM (corresponding to the mass ratio of TPGS to MCS from 0.1 to 0.3), the $D_{\text{h},\text{v}}$ values of CSNCs gradually decreased from 200 ± 8 to 57 ± 3 nm whereas the PDI values of CSNCs increased from 0.13 ± 0.03 to 0.26 ± 0.01 (Table 1). Moreover, the presence of TPGS also resulted in a higher cross-linking efficiency of CSNCs, and the conversions of *N*-maleoyl groups reached 77–78%. For instance, the ^1H NMR spectrum of CSNC-3 ($[\text{TPGS}] = 0.54$ mM) showed very weak remaining resonances of *N*-maleoyl protons at 5.82 and 6.36 ppm, illustrating a relatively high cross-linking efficiency (Figure 1b). The enhanced conversions can be attributed to the increased transparency of respective miniemulsions, which allowed more effective penetration of UV light into the cross-linking systems. TEM was utilized to verify the structural features of CSNCs. CSNC-2 was selected as a representative sample because its size allows for the ready observation of the capsular structure. In a good agreement with the hydrodynamic size distribution of CSNC-2 in aqueous solution as detected by DLS (Figure S1), CSNC-2 showed surface sizes ranging from ~50 to ~400 nm on the TEM grid. Figure 2 illustrates the TEM image of several individual capsules of CSNC-2 with surface sizes greater than 100 nm. They exhibited a well-defined hollow structure with a shell thickness of about 20 nm, providing direct experimental evidence for the formation of capsules from CS-based material by using the miniemulsion interfacial cross-linking approach. Grainlike shell morphology was observed for CSNC-2, presumably because of the high rigidity of the polymer chain of MCS. Because the dimension of ~10 nm for each grainlike domain is close to the average length of CS_{5k}-based backbones of MCS molecules (mass per unit length of CS = 450 ± 20 Da/nm),⁵² the results may indicate that each grainlike domain was

Table 1. Preparation of CSNCs with Tunable Sizes^a

entry	TPGS (mM)	conversion (%) ^b	$D_{\text{h},\text{v}}$ (nm) ^c	PDI ^c
CSNC-0	0	64	388 ± 29	0.14 ± 0.02
CSNC-1	0.18	77	200 ± 8	0.13 ± 0.03
CSNC-2	0.37	78	130 ± 9	0.20 ± 0.03
CSNC-3	0.54	78	57 ± 3	0.26 ± 0.01

^aPreparation conditions: $[\text{ene}]_0/[\text{SH}]_0/[\text{DMPA}]_0 = 1:1:0.5$, 3 vol % chloroform in water, 6 wt % MCS relative to chloroform, room temperature, 20 min of ultrasonication, and 1 h of UV irradiation. ^bBy ^1H NMR analysis. ^cBy DLS analysis.

labile β -thiopropionate cross-linkages for the CSNCs,⁴⁴ 1,4-butanediol bis(3-mercaptopropionate) was selected as the cross-linker.^{40,41} To accelerate the thiol–ene cross-linking process, 2,2-dimethoxy-2-phenylacetophenone (DMPA) was used as the photoinitiator ($[\text{N-maleoyl}]_0/[\text{SH}]_0/[\text{DMPA}]_0 = 1:1:0.5$).⁵⁰ To PEGylate CSNCs and to exert size control over CSNCs, TPGS was used as the cosurfactant because of its biocompatible and nontoxic properties.⁵¹

As a control experiment, the synthesis of CSNCs was conducted in the absence of TPGS, using 6 wt % MCS relative to chloroform ($W_{\text{water}}/W_{\text{chloroform}} = 21$). After 20 min of ultrasonication, a translucent miniemulsion was obtained. Subsequently, an interfacial thiol–ene cross-linking reaction was induced for 1 h with UV irradiation ($\lambda_{\text{max}} = 365$ nm), followed by the complete removal of chloroform. As shown by DLS analysis, CSNC-0 had a volume-average hydrodynamic diameter ($D_{\text{h},\text{v}}$) of 388 ± 29 nm and a polydispersity (PDI) of 0.14 ± 0.02 . According to its hydrodynamic size, CSNC-0 may not be suitable for long circulation because of clearance through the reticuloendothelial system.²⁸ Because the alkene functionalities in *N*-maleoyl groups are 1,2-disubstituted, the formation of sulfur–carbon bonds between the sulfur atoms from thiol groups of cross-linker and either carbon atom of the alkene units can be feasible. ^1H NMR analysis further indicated that 64% of *N*-maleoyl groups from MCS were cross-linked on the basis of the resonance intensities of the remaining *N*-maleoyl alkene protons. Because theoretically the maximum possible conversion of *N*-maleoyl groups was 100% according to the $[\text{N-maleoyl}]_0/[\text{SH}]_0$ feed ratio, the limited experimental con-

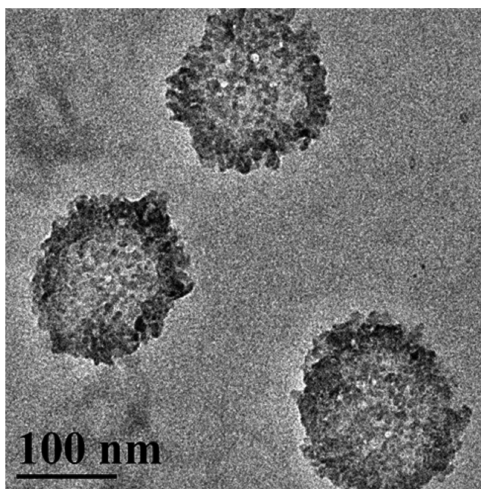


Figure 2. TEM image of CSNC-2.

formed by many cross-linked rodlike MCS polymer chains whereas these grainlike domains were also covalently linked. Because of the grainlike shell morphology of CSNCs and the limited TEM resolution, smaller CSNCs could not be visualized clearly by TEM. According to the DLS analysis of their hydrodynamic sizes, all CSNCs showed good colloidal stability in water and phosphate buffer solutions, without a significant occurrence of aggregation. However, the scattering intensity of CSNCs can decrease more substantially in pH 5.5 buffer than in pH 7.4 buffer. For instance, the average relative intensity (I/I_0) of CSNC-3 at pH 5.5 dropped to 45% of the initial value after 7 days whereas I/I_0 remained essentially unchanged at pH 7.4 after the same incubation time (Figure S2). Because the scattering intensity is positively correlated with the molar mass of CSNCs, the result can be ascribed to the mass loss from CSNCs resulting from the acid-triggered cleavage of the cross-linkages. Additionally, these CSNCs possess significant positive charge (with a ζ potential of up to ~ 30 mV) under acidic conditions as a result of the protonation of the primary amine groups on their CS-based polymer chains.

Although the utilization of cosurfactant may facilitate the preparation of CSNCs with reduced sizes, a high concentration of cosurfactant should be avoided because the presence of excess cosurfactant at the interface can sterically hinder the occurrence of the cross-linking reaction. For instance, when the TPGS concentration was further increased to 0.9 mM with other reaction conditions unchanged, a decreased extent of reaction (71%) of *N*-maleoyl groups was observed, and DLS analysis indicated the formation of cross-linked nanostructures with $D_{h,v} = 28 \pm 4$ nm, but TEM characterization was unable to identify their capsular structures. In addition, the large PDI value (0.57 ± 0.04) of these cross-linked nanostructures suggested poor template control during the cross-linking reaction.

Encapsulation of the anticancer drug using the CSNCs was further studied. As a potent antitumor agent with UV-vis and fluorescence signals, Dox was selected as the representative anticancer drug in this study. Dox-CSNCs were prepared by the *in situ* encapsulation of Dox during the miniemulsion cross-linking process. With their average nanoscopic dimensions in or close to the size range for long circulation,²⁸ CSNC-2 and CSNC-3 were selected as the optimal formulations for drug encapsulation. The preparation of Dox-CSNCs was conducted following the same procedure for the synthesis of CSNCs,

except for the addition of Dox to oil droplets (7.4 wt % relative to CSNCs) prior to ultrasonication and the removal of free Dox from the water phase via extraction after miniemulsion cross-linking. With a high cross-linking efficiency, Dox-CSNCs were obtained as red, transparent aqueous solutions. As measured by DLS, the hydrodynamic sizes and PDI values of Dox-CSNC-2 ($D_{h,v} = 143 \pm 8$ nm, PDI = 0.22 ± 0.01) and Dox-CSNC-3 ($D_{h,v} = 65 \pm 6$ nm, PDI = 0.24 ± 0.01) were similar to those of CSNC-2 ($D_{h,v} = 130 \pm 9$ nm; PDI = 0.20 ± 0.03) and CSNC-3 ($D_{h,v} = 57 \pm 3$ nm; PDI = 0.26 ± 0.01), indicating that the presence of Dox would not considerably affect the miniemulsion cross-linking systems. According to analysis by UV-vis spectroscopy, 6.1 wt % Dox relative to CSNC-2 was eventually encapsulated in Dox-CSNC-2, corresponding to an 82% encapsulation efficiency; similarly, 5.6 wt % Dox relative to CSNC-3 was eventually encapsulated in Dox-CSNC-3, corresponding to a 76% encapsulation efficiency. Although the Dox encapsulation process was not optimized to maximize the loading, such a Dox loading level in CSNCs is higher than that in CS-based nanoparticles. As reported by Alonso and co-workers,⁵³ the Dox loading level in CS-based nanoparticles via a typical encapsulation approach is very low, and they successfully achieved up to 4.0 wt % Dox loading in CS-based nanoparticles through a modified encapsulation method via complexing Dox and a polyanion at first. Relative to CS-based nanoparticles, CSNCs can readily encapsulate a larger amount of Dox for two reasons. First, significant amounts of Dox can be encapsulated by the cavities in CSNCs. Second, Dox encapsulation by CSNCs can be readily performed in neutral aqueous solution, but Dox encapsulation by CS-based nanoparticles typically needs to be conducted under acidic conditions in which there is unfavorable electrostatic repulsion between protonated Dox and CS.⁵³

Drug Release of Dox-CSNCs. To assess the applicability of CSNCs in the delivery of anticancer drugs, Dox release behavior of Dox-CSNC-2 and Dox-CSNC-3 was probed in phosphate buffer solutions at pH 7.4 and 5.5 using a dialysis approach (MWCO of dialysis membrane = 3500 Da). These pH values were chosen because pH 7.4 represents the typical acidity of the bloodstream and normal tissue, and pH 5.5 represents the average acidity of intracellular endosome and lysosome (pH range = 4.5–6.5).⁵⁴ Three important phenomena of Dox release from Dox-CSNCs were observed (Figure 3).

First, as expected, these Dox-CSNCs exhibited a significantly enhanced Dox release rate at pH 5.5 as compared to that at pH 7.4. Dox release amounts after 48 h of incubation increased

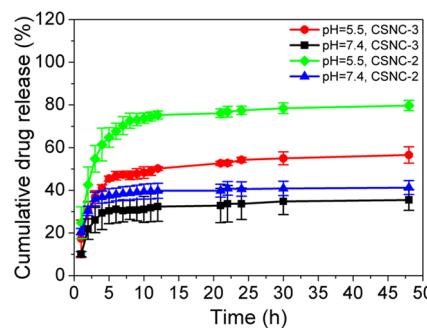


Figure 3. In vitro Dox release profiles of Dox-CSNC-2 and Dox-CSNC-3 in pH 7.4 and pH 5.5 buffer solutions at 37 °C. Error bars in drug release experiments represent standard deviation values resulting from three independent experiments.

from 41% at pH 7.4 to 80% at pH 5.5 for Dox-CSNC-2 and from 35% at pH 7.4 to 57% at pH 5.5 for Dox-CSNC-3. The increase in the Dox release rates and accumulative amounts at pH 5.5 can be attributed to the appreciable hydrolytic cleavage of β -thiopropionate cross-linkages at more acidic pH,⁴⁴ which facilitates the formation of a more permeable wall structure of the NCs. The steady decrease in the scattering intensity of CSNCs at pH 5.5 with the increase in incubation time further suggested that Dox diffusion resistance would decrease during the release process as a result of the mass loss of the shell resulting from the acid-triggered cleavage of cross-linkages (Figure S2). Additionally, the increase in the solubility of Dox under acidic conditions may also promote Dox release from CSNCs. Fritze et al. reported a 4.5-fold increase in Dox solubility with a decrease in pH, from 0.0625 mg/mL at pH 7.4 to \sim 0.28 mg/mL at pH 5.5 in phosphate buffer.⁵⁵ Although the initial average Dox concentration of 0.0124 mg/mL in our drug release studies was relatively low, the local concentration of Dox could be much higher, particularly under acidic conditions, thereby boosting the Dox release rate at pH 5.5.

Second, faster Dox release from Dox-CSNC-2 relative to that from Dox-CSNC-3 was demonstrated. This result might be ascribed to the composition and structural differences of shells of these CSNCs. There was a higher concentration of cosurfactant TPGS in Dox-CSNC-3 than in Dox-CSNC-2. Relative to the grainlike domains with densely packed CS-based polymer chains, the intergrain areas on the shell of NCs are expected to have a lower diffusion resistance. However, a significant presence of cosurfactant TPGS in the intergrain interfacial areas can be expected, and the diffusion resistance of such areas may increase with an increase in TPGS concentration.

Third, both Dox-CSNC-2 and Dox-CSNC-3 showed two phases of Dox release, with relatively fast release in the first several hours and very slow release afterward. Because the miniemulsion-based approach was used for Dox encapsulation and the physical absorption of Dox on the outer surface of CSNCs would be negligible, there should be a significant presence of Dox encapsulated in both the shells and inner cavities of CSNCs before release. The first phase of Dox release may mostly correspond to the Dox moieties encapsulated in the shells of CSNCs, especially in the outer layers of shells, as a result of the low diffusion path length and resistance. Environmental acidity can have a critical influence on Dox release in this phase. It should also be noted that, because of the presence of the polymeric scaffold, the first phase of Dox release from CSNCs is still evidently slower than the diffusion of free Dox from the dialysis bag.⁵⁶ The second phase of Dox release might be partially attributed to the remarkable diffusion resistance of Dox moieties entrapped in the central cavity of CSNCs and encapsulated in the inner layers of the shells of CSNCs. Other factors, such as the formation of chemical and physical Dox aggregates, may also contribute to the retardation of the Dox release.⁵⁷ Specific interactions of Dox with CS-based polymer scaffolds via H-bonding may slow down the release of Dox, especially at a pH of 7.4.⁵⁷ It appears that Dox release in this phase is less sensitive to environmental acidity. Therefore, it is possible that the enhanced electrostatic repulsion under acidic conditions between the protonated shells of CSNCs and the protonated Dox moieties entrapped in the cavities may also considerably retard Dox release.

It was previously reported that tumor tissues exhibit a more acidic microenvironment (with pH values as low as 5.7) than

do normal tissues, which is caused in part by the accumulation of lactic acid resulting from anaerobic glucose metabolism.¹² To this end, CSNCs can have benefits for delivering a variety of hydrophobic anticancer drugs to acidic tumor tissues with a high local concentration because of its pH-dependent release features, thus effectively minimizing the adverse effects resulting from drugs.

Cytotoxicity and Cellular Uptake of Dox-CSNC-3. With well-defined PEGylated capsular nanostructures and a pH-responsive drug release profile, Dox-CSNC-3 was further assessed through in vitro cytotoxicity and cell uptake studies. The MCF-7 breast cancer cell line was selected as the experimental model for cancer cells. The MTS assay for cell viability was utilized in the in vitro cytotoxicity analysis. As compared to free Dox, Dox-CSNC-3 exhibited even higher therapeutic efficacy in killing MCF-7 cells over the entire concentration range of Dox moieties ($[Dox]_0 = 0.1\text{--}5 \mu\text{g/mL}$) after 48 h of incubation (Figure 4). The cytotoxicity

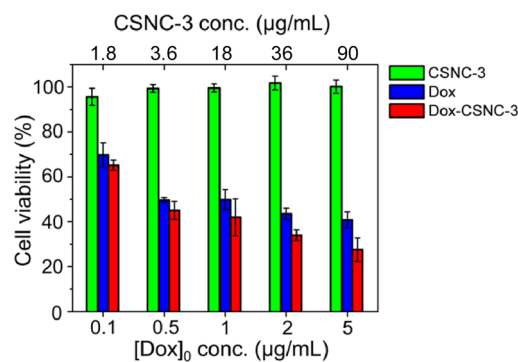


Figure 4. Cytotoxicity assessments of CSNC-3, Dox, and Dox-CSNC-3 toward MCF-7 cells (after 48 h of incubation). Error bars represent standard deviation values resulting from three independent experiments.

enhancement of Dox-CSNC-3 relative to free Dox was minimal at lower Dox concentration levels (0.1 to 1 $\mu\text{g/mL}$) but became more noticeable at higher concentrations (2 to 5 $\mu\text{g/mL}$). For example, at Dox concentrations of 2 and 5 $\mu\text{g/mL}$, the cell viability was decreased from 44 to 34% and from 41 to 27%, respectively, as a result of the scaffold effects of CSNCs. However, as the negative control, the empty CSNC-3 did not show considerable cytotoxicity against the MCF-7 cell line at all experimental concentrations (1.8 to 90 $\mu\text{g/mL}$), indicating the remarkable biocompatibility of the scaffold.

To visualize the delivery of Dox via NCs in cancer cells, using free Dox as a control, Dox-CSNC-3 was incubated in MCF-7 cells for 1 and 4 h at 37 °C, followed by the observation of fluorescence (red) signals from Dox using confocal laser scanning microscopy (Figure 5a). Only weak Dox fluorescence could be observed within cells after 1 h of incubation; however, Dox fluorescence in the cytoplasmic space and the nucleus of cells became much stronger after 4 h of incubation. In the control experiment (Figure 5b), free Dox was immediately taken up by MCF-7 cells after 1 h of incubation, and significant Dox fluorescence within cells was observed. However, relative to 1 h of incubation, 4 h of incubation with free Dox resulted in only a moderate increase in the Dox fluorescence intensity within cells, indicating that the intracellular accumulation of free Dox became slow after a short period of incubation. The above results can be explained through different cellular uptake

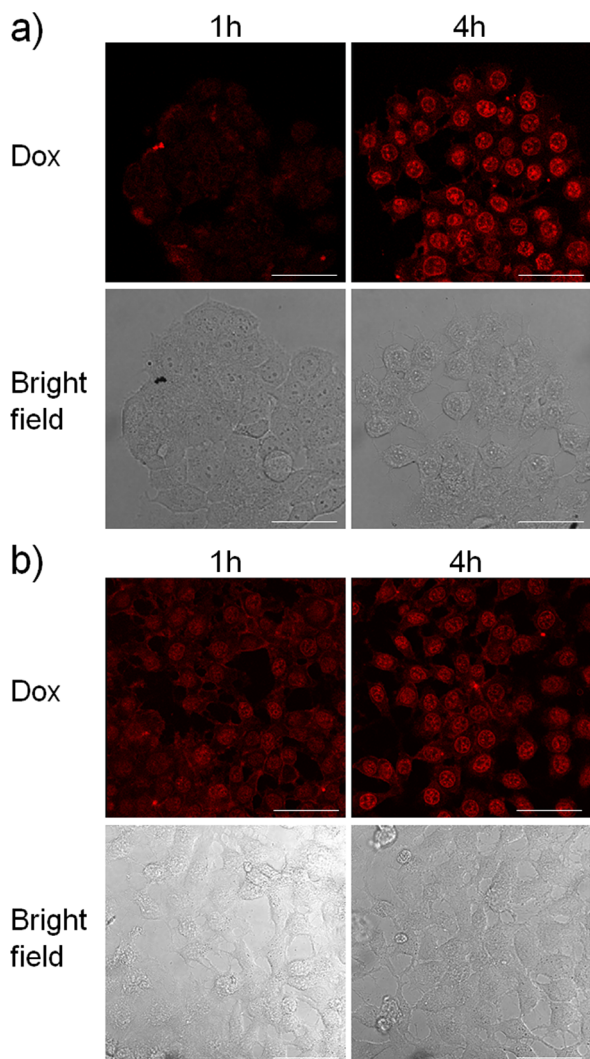


Figure 5. Confocal images of MCF-7 cells treated for 1 and 4 h with (a) Dox-CSNC-3 and (b) free Dox. Scale bar = 46.72 μm .

mechanisms for Dox-CSNC-3 and free Dox. Dox-CSNC-3 was taken up through an endocytosis mechanism, and the electrostatic interaction between their positively charged surface (ζ -potential: 5 mV at pH 7.4 and 31 mV at pH 5.5) and negatively charged cell membranes may further facilitate the internalization process.^{2,58} In contrast, the cellular internalization of Dox primarily relies on a passive diffusion mechanism,³² and the driving force for the uptake process keeps on decreasing because of the decreased Dox concentration difference across the cell membrane during incubation.

The results from cytotoxicity and cellular uptake studies further suggested that the presence of CSNCs as delivery scaffolds may slow the diffusion of Dox out of cells and help to maintain a higher intracellular Dox concentration for an extended period of time, thereby leading to enhanced therapeutic effects of Dox toward MCF-7 cells. Before the internalization of Dox-CSNC-3, Dox release should be minimal because of the physiological pH of the cell culture media. However, intracellular Dox release from CSNCs can be significant because of the acidic environments within intracellular endosomes and lysosomes (pH 4.5–6.5).⁵⁴ Because Dox is known to kill cancer cells by intercalating DNA and inhibiting the progression of DNA polymerase and topoisomer-

ase II,⁵⁹ it can also be deduced that the significant accumulation of Dox in nucleus sites via CSNCs led to the apoptosis of treated cancer cells, thus resulting in enhanced antitumor efficacy.

CONCLUSIONS

We have demonstrated that well-defined CSNCs with tunable sizes can be readily prepared by the UV-induced thiol–ene miniemulsion cross-linking of MCS. Dox, as a representative hydrophobic anticancer drug, can be readily encapsulated in situ by the CSNCs. Through the incorporation of acid-labile β -thiopropionate cross-linkages, Dox-loaded CSNCs exhibited a faster release of Dox at pH 5.5 than at pH 7.4. Although CSNCs have no considerable cytotoxicity, Dox can be effectively delivered to MCF-7 cancer cells by using CSNCs as delivery scaffolds, resulting in enhanced cytotoxicity. On the basis of the synthetic approach developed in this work, a broad variety of anticancer hydrophobic drugs may be loaded into the CSNCs for selective drug release in acidic tumor tissues. The in vitro results obtained in this work suggest that anticancer drug formulations using CSNCs as delivery scaffolds have promising applications in cancer treatment.

ASSOCIATED CONTENT

Supporting Information

Representative DLS histograms of the CSNCs in deionized water. Time dependence of relative intensity of scattered light of CSNC-3. This material is available free of charge via the Internet at <http://pubs.acs.org>.

AUTHOR INFORMATION

Corresponding Author

*Phone: 716-645-1193. Fax: 716-645-3822. E-mail: ccheng8@buffalo.edu.

Present Address

(W.-C.L.) Department of Industrial and Systems Engineering, The Hong Kong Polytechnic University, Hung Hom, Kowloon, Hong Kong, PR China.

Notes

The authors declare no competing financial interest.

ACKNOWLEDGMENTS

We are grateful for NSF grants (CBET-1133737 and DMR-1206715) and a SUNY—Buffalo Schomburg fellowship (C.H.J.) for financial support.

REFERENCES

- Ademuyiwa, F. O.; Edge, S. B.; Erwin, D. O.; Orom, H.; Ambrosone, C. B.; Underwood, W. Breast Cancer Racial Disparities: Unanswered Questions. *Cancer Res.* **2011**, *71*, 640–644.
- Khan, M.; Ong, Z. Y.; Wiradharma, N.; Attia, A. B. E.; Yang, Y.-Y. Advanced Materials for Co-Delivery of Drugs and Genes in Cancer Therapy. *Adv. Healthcare Mater.* **2012**, *1*, 373–392.
- Lee, Y.; Graeser, R.; Kratz, F.; Geckeler, K. E. Paclitaxel-Loaded Polymer Nanoparticles for the Reversal of Multidrug Resistance in Breast Cancer Cells. *Adv. Funct. Mater.* **2011**, *21*, 4211–4218.
- Shi, J.; Votruba, A. R.; Farokhzad, O. C.; Langer, R. Nanotechnology in Drug Delivery and Tissue Engineering: From Discovery to Applications. *Nano Lett.* **2010**, *10*, 3223–3230.
- Elsabahy, M.; Wooley, K. L. Design of Polymeric Nanoparticles for Biomedical Delivery Applications. *Chem. Soc. Rev.* **2012**, *41*, 2545–2561.
- Ge, Z.; Liu, S. Functional Block Copolymer Assemblies Responsive to Tumor and Intracellular Microenvironments for Site-

- Specific Drug Delivery and Enhanced Imaging Performance. *Chem. Soc. Rev.* **2013**, *42*, 7289–7325.
- (7) Duncan, R.; Gaspar, R. Nanomedicine(s) under the Microscope. *Mol. Pharmaceutics* **2011**, *8*, 2101–2141.
- (8) Duncan, R.; Richardson, S. C. W. Endocytosis and Intracellular Trafficking as Gateways for Nanomedicine Delivery: Opportunities and Challenges. *Mol. Pharmaceutics* **2012**, *9*, 2380–2402.
- (9) Yu, Y.; Chen, C.-K.; Law, W.-C.; Mok, J.; Zou, J.; Prasad, P. N.; Cheng, C. Well-Defined Degradable Brush Polymer–Drug Conjugates for Sustained Delivery of Paclitaxel. *Mol. Pharmaceutics* **2012**, *10*, 867–874.
- (10) Zou, J.; Yu, Y.; Yu, L.; Li, Y. K.; Chen, C. K.; Cheng, C. Well-Defined Drug-Conjugated Biodegradable Nanoparticles by Azide-Alkyne Click Crosslinking in Miniemulsion. *J. Polym. Sci., Part A: Polym. Chem.* **2012**, *50*, 142–148.
- (11) Gao, W.; Chan, J. M.; Farokhzad, O. C. pH-Responsive Nanoparticles for Drug Delivery. *Mol. Pharmaceutics* **2010**, *7*, 1913–1920.
- (12) Vaupel, P. Tumor Microenvironmental Physiology and Its Implications for Radiation Oncology. *Semin. Radiat. Oncol.* **2004**, *14*, 198–206.
- (13) Kumar, M. N. V. R.; Muzzarelli, R. A. A.; Muzzarelli, C.; Sashiwa, H.; Domb, A. J. Chitosan Chemistry and Pharmaceutical Perspectives. *Chem. Rev.* **2004**, *104*, 6017–6084.
- (14) Agnihotri, S. A.; Mallikarjuna, N. N.; Aminabhavi, T. M. Recent Advances on Chitosan-Based Micro- and Nanoparticles in Drug Delivery. *J. Controlled Release* **2004**, *100*, 5–28.
- (15) Cui, D.; Szarpak, A.; Pignot-Paintrand, I.; Varrot, A.; Boudou, T.; Detrembleur, C.; Jérôme, C.; Picart, C.; Auzély-Vely, R. Contact-Killing Polyelectrolyte Microcapsules Based on Chitosan Derivatives. *Adv. Funct. Mater.* **2010**, *20*, 3303–3312.
- (16) Hua, D. B.; Jiang, J. L.; Kuang, L. J.; Jiang, J.; Zheng, W.; Liang, H. J. Smart Chitosan-Based Stimuli-Responsive Nanocarriers for the Controlled Delivery of Hydrophobic Pharmaceuticals. *Macromolecules* **2011**, *44*, 1298–1302.
- (17) Du, C.; Zhao, J.; Fei, J.; Cui, Y.; Li, J. Assembled Microcapsules by Doxorubicin and Polysaccharide as High Effective Anticancer Drug Carriers. *Adv. Healthcare Mater.* **2013**, 1246–1251.
- (18) Ping, Y. A.; Liu, C. D.; Tang, G. P.; Li, J. S.; Li, J.; Yang, W. T.; Xu, F. J. Functionalization of Chitosan via Atom Transfer Radical Polymerization for Gene Delivery. *Adv. Funct. Mater.* **2010**, *20*, 3106–3116.
- (19) Amoozgar, Z.; Park, J. Y.; Lin, Q. N.; Yeo, Y. Low Molecular-Weight Chitosan as a pH-Sensitive Stealth Coating for Tumor-Specific Drug Delivery. *Mol. Pharmaceutics* **2012**, *9*, 1262–1270.
- (20) Lallana, E.; Fernandez-Megia, E.; Riguera, R. Surpassing the Use of Copper in the Click Functionalization of Polymeric Nanostructures: A Strain-Promoted Approach. *J. Am. Chem. Soc.* **2009**, *131*, 5748–5750.
- (21) Bulwan, M.; Zapotoczny, S.; Nowakowska, M. Robust “One-Component” Chitosan-Based Ultrathin Films Fabricated Using Layer-by-Layer Technique. *Soft Matter* **2009**, *5*, 4726–4732.
- (22) Verheul, R. J.; van der Wal, S.; Hennink, W. E. Tailorable Thiolated Trimethyl Chitosans for Covalently Stabilized Nanoparticles. *Biomacromolecules* **2010**, *11*, 1965–1971.
- (23) Lee, C. M.; Jang, D.; Kim, J.; Cheong, S. J.; Kim, E. M.; Jeong, M. H.; Kim, S. H.; Kim, D. W.; Lim, S. T.; Sohn, M. H.; Jeong, Y. Y.; Jeong, H. J. Oleyl-Chitosan Nanoparticles Based on a Dual Probe for Optical/MR Imaging in Vivo. *Bioconjugate Chem.* **2011**, *22*, 186–192.
- (24) Prabaharan, M.; Grailer, J. J.; Steeber, D. A.; Gong, S. Q. Stimuli-Responsive Chitosan-graft-poly(N-vinylcaprolactam) as a Promising Material for Controlled Hydrophobic Drug Delivery. *Macromol. Biosci.* **2008**, *8*, 843–851.
- (25) Zhao, Z. M.; He, M.; Yin, L. C.; Bao, J. M.; Shi, L. L.; Wang, B. Q.; Tang, C.; Yin, C. H. Biodegradable Nanoparticles Based on Linoleic Acid and Poly(β -malic acid) Double Grafted Chitosan Derivatives as Carriers of Anticancer Drugs. *Biomacromolecules* **2009**, *10*, 565–572.
- (26) Zhou, H. F.; Yu, W. T.; Guo, X.; Liu, X. D.; Li, N.; Zhang, Y.; Ma, X. J. Synthesis and Characterization of Amphiphilic Glycidol-Chitosan-Deoxycholic Acid Nanoparticles as a Drug Carrier for Doxorubicin. *Biomacromolecules* **2010**, *11*, 3480–3486.
- (27) Xu, J. H.; Zhao, H.; Lan, W. J.; Luo, G. S. A Novel Microfluidic Approach for Monodispersed Chitosan Microspheres with Controllable Structures. *Adv. Healthcare Mater.* **2012**, *1*, 106–111.
- (28) Petros, R. A.; DeSimone, J. M. Strategies in the Design of Nanoparticles for Therapeutic Applications. *Nat. Rev. Drug Discov.* **2010**, *9*, 615–627.
- (29) Wei, W.; Yuan, L.; Hu, G.; Wang, L. Y.; Wu, H.; Hu, X.; Su, Z. G.; Ma, G. H. Monodisperse Chitosan Microspheres with Interesting Structures for Protein Drug Delivery. *Adv. Mater.* **2008**, *20*, 2292–2296.
- (30) Zeiger, E.; Gollapudi, B.; Spencer, P. Genetic Toxicity and Carcinogenicity Studies of Glutaraldehyde - A Review. *Mutat. Res., Rev. Mutat. Res.* **2005**, *589*, 136–151.
- (31) Hu, Y.; Jiang, X. Q.; Ding, Y.; Chen, Q.; Yang, C. Z. Core-Template-Free Strategy for Preparing Hollow Nanospheres. *Adv. Mater.* **2004**, *16*, 933–937.
- (32) Hu, Y.; Ding, Y.; Ding, D.; Sun, M. J.; Zhang, L. Y.; Jiang, X. Q.; Yang, C. Z. Hollow Chitosan/Poly(acrylic acid) Nanospheres as Drug Carriers. *Biomacromolecules* **2007**, *8*, 1069–1076.
- (33) Peng, X. H.; Zhang, L. Surface Fabrication of Hollow Microspheres from N-Methylated Chitosan Cross-Linked with Glutaraldehyde. *Langmuir* **2005**, *21*, 1091–1095.
- (34) Mi, F.-L.; Wu, Y.-Y.; Lin, Y.-H.; Sonaje, K.; Ho, Y.-C.; Chen, C.-T.; Juang, J.-H.; Sung, H.-W. Oral Delivery of Peptide Drugs Using Nanoparticles Self-Assembled by Poly(γ -glutamic acid) and a Chitosan Derivative Functionalized by Trimethylation. *Bioconjugate Chem.* **2008**, *19*, 1248–1255.
- (35) Payet, L.; Terentjev, E. M. Emulsification and Stabilization Mechanisms of O/W Emulsions in the Presence of Chitosan. *Langmuir* **2008**, *24*, 12247–12252.
- (36) Liu, L.; Yang, J. P.; Ju, X. J.; Xie, R.; Liu, Y. M.; Wang, W.; Zhang, J. J.; Niu, C. H.; Chu, L. Y. Monodisperse Core-Shell Chitosan Microcapsules for pH-Responsive Burst Release of Hydrophobic Drugs. *Soft Matter* **2011**, *7*, 4821–4827.
- (37) Alexis, F.; Pridgen, E.; Molnar, L. K.; Farokhzad, O. C. Factors Affecting the Clearance and Biodistribution of Polymeric Nanoparticles. *Mol. Pharmaceutics* **2008**, *5*, 505–515.
- (38) Marie, E.; Landfester, K.; Antonietti, M. Synthesis of Chitosan-Stabilized Polymer Dispersions, Capsules, and Chitosan Grafting Products via Miniemulsion. *Biomacromolecules* **2002**, *3*, 475–481.
- (39) Zhang, W. J.; Gilstrap, K.; Wu, L. Y.; Bahadur, K. C. R.; Moss, M. A.; Wang, Q. A.; Lu, X. B.; He, X. M. Synthesis and Characterization of Thermally Responsive Pluronic F127-Chitosan Nanocapsules for Controlled Release and Intracellular Delivery of Small Molecules. *ACS Nano* **2010**, *4*, 6747–6759.
- (40) Zou, J.; Hew, C. C.; Themistou, E.; Li, Y. K.; Chen, C. K.; Alexandridis, P.; Cheng, C. Clicking Well-Defined Biodegradable Nanoparticles and Nanocapsules by UV-Induced Thiol-Ene Cross-Linking in Transparent Miniemulsions. *Adv. Mater.* **2011**, *23*, 4274–4277.
- (41) Chen, C.-K.; Law, W.-C.; Aalinkeel, R.; Nair, B.; Yu, Y.; Mahajan, S. D.; Reynolds, J. L.; Wu, J.; Li, Y.; Lai, C. K.; Tzanakakis, E. S.; Schwartz, S. A.; Prasad, P. N.; Cheng, C. Biodegradable Cationic Polymer Nanocapsules for Bypassing Multidrug Resistance and Enabling Drug-Gene Co-Delivery to Cancer Cells. *Nanoscale* **2014**, *6*, 1567–1572.
- (42) Li, Y.; Themistou, E.; Das, B. P.; Christian-Tabak, L.; Zou, J.; Tsianou, M.; Cheng, C. Polyelectrolyte Nanocages via Crystallized Miniemulsion Droplets. *Chem. Commun.* **2011**, *47*, 11697–11699.
- (43) Oishi, M.; Sasaki, S.; Nagasaki, Y.; Kataoka, K. pH-Responsive Oligodeoxynucleotide (ODN)-Poly(ethylene glycol) Conjugate through Acid-Labile β -Thiopropionate Linkage: Preparation and Polyion Complex Micelle Formation. *Biomacromolecules* **2003**, *4*, 1426–1432.

- (44) Zou, J.; Zhang, F.; Zhang, S.; Pollack, S. F.; Elsabahy, M.; Fan, J.; Wooley, K. L. Poly(ethylene oxide)-block-Polyphosphoester-graft-Paclitaxel Conjugates with Acid-Labile Linkages as a pH-Sensitive and Functional Nanoscopic Platform for Paclitaxel Delivery. *Adv. Healthcare Mater.* **2014**, *3*, 441–448.
- (45) Benoit, D. S. W.; Henry, S. M.; Shubin, A. D.; Hoffman, A. S.; Stayton, P. S. pH-Responsive Polymeric siRNA Carriers Sensitize Multidrug Resistant Ovarian Cancer Cells to Doxorubicin via Knockdown of Polo-Like Kinase 1. *Mol. Pharmaceutics* **2010**, *7*, 442–455.
- (46) Lu, B.; Xu, X.-D.; Zhang, X.-Z.; Cheng, S.-X.; Zhuo, R.-X. Low Molecular Weight Polyethylenimine Grafted N-Maleated Chitosan for Gene Delivery: Properties and in Vitro Transfection Studies. *Biomacromolecules* **2008**, *9*, 2594–2600.
- (47) Kasaai, M. R. Determination of the Degree of N-Acetylation for Chitin and Chitosan by Various NMR Spectroscopy Techniques: A Review. *Carbohydr. Polym.* **2010**, *79*, 801–810.
- (48) Zhong, C.; Wu, J.; Reinhart-King, C. A.; Chu, C. C. Synthesis, Characterization and Cytotoxicity of Photo-Crosslinked Maleic Chitosan-Polyethylene Glycol Diacrylate Hybrid Hydrogels. *Acta Biomater.* **2010**, *6*, 3908–3918.
- (49) Chen, C.-K.; Law, W.-C.; Aalinkeel, R.; Nair, B.; Kopwitthaya, A.; Mahajan, S. D.; Reynolds, J. L.; Zou, J.; Schwartz, S. A.; Prasad, P. N.; Cheng, C. Well-Defined Degradable Cationic Polylactide as Nanocarrier for the Delivery of siRNA to Silence Angiogenesis in Prostate Cancer. *Adv. Healthcare Mater.* **2012**, *1*, 751–761.
- (50) Campos, L. M.; Killops, K. L.; Sakai, R.; Paulusse, J. M. J.; Damiron, D.; Drockenmuller, E.; Messmore, B. W.; Hawker, C. J. Development of Thermal and Photochemical Strategies for Thiol–Ene Click Polymer Functionalization. *Macromolecules* **2008**, *41*, 7063–7070.
- (51) Liu, Y.; Huang, L.; Liu, F. Paclitaxel Nanocrystals for Overcoming Multidrug Resistance in Cancer. *Mol. Pharmaceutics* **2010**, *7*, 863–869.
- (52) Morris, G. A.; Castile, J.; Smith, A.; Adams, G. G.; Harding, S. E. Macromolecular Conformation of Chitosan in Dilute Solution: A New Global Hydrodynamic Approach. *Carbohydr. Polym.* **2009**, *76*, 616–621.
- (53) Janes, K. A.; Fresneau, M. P.; Marazuela, A.; Fabra, A.; Alonso, M. J. Chitosan Nanoparticles as Delivery Systems for Doxorubicin. *J. Controlled Release* **2001**, *73*, 255–267.
- (54) Schmaljohann, D. Thermo- and pH-Responsive Polymers in Drug Delivery. *Adv. Drug Delivery Rev.* **2006**, *58*, 1655–1670.
- (55) Fritze, A.; Hens, F.; Kimpfler, A.; Schubert, R.; Peschka-Süss, R. Remote Loading of Doxorubicin into Liposomes Driven by a Transmembrane Phosphate Gradient. *Biochim. Biophys. Acta* **2006**, *1758*, 1633–1640.
- (56) Yueying, H.; Yan, Z.; Chunhua, G.; Weifeng, D.; Meidong, L. Micellar Carrier Based on Methoxy Poly(ethylene glycol)-block-poly(ϵ -caprolactone) Block Copolymers Bearing Ketone Groups on the Polyester Block for Doxorubicin Delivery. *J. Mater. Sci.: Mater. Med.* **2010**, *21*, 567–574.
- (57) Sutton, D.; Wang, S.; Nasongkla, N.; Gao, J.; Dormidontova, E. E. Doxorubicin and β -Lapachone Release and Interaction with Micellar Core Materials: Experiment and Modeling. *Exp. Biol. Med.* **2007**, *232*, 1090–1099.
- (58) Jones, C. H.; Chen, C.-K.; Jiang, M.; Fang, L.; Cheng, C.; Pfeifer, B. A. Synthesis of Cationic Polylactides with Tunable Charge Densities as Nanocarriers for Effective Gene Delivery. *Mol. Pharmaceutics* **2013**, *10*, 1138–1145.
- (59) Fornari, F. A.; Randolph, J. K.; Yalowich, J. C.; Ritke, M. K.; Gewirtz, D. A. Interference by Doxorubicin with DNA Unwinding in MCF-7 Breast Tumor Cells. *Mol. Pharmacol.* **1994**, *45*, 649–656.